ACS Partner Journal

CHEM & BIO ENGINEERING

Editors' Choice

Open Access

pubs.acs.org/ChemBioEng

Article

Programmable Cargo Release from Jet-Printed Microgel Particles via an In Situ Ionic Exchange Method

Rong Ma,[¶] Jihpeng Sun,[¶] Sungwan Park, Fiona Nikolla, and Albert Tianxiang Liu*

Cite This: https://doi.org/10.1021/cbe.5c00017

Read Online

ACCESS | Metrics & More | Article Recommendations | Supporting Information

ABSTRACT: Hydrogel-based drug delivery systems hold significant clinical potential by enabling precise spatial and temporal control over therapeutic release, ranging from metabolites, macromolecules to other cellular and subcellular constructs. However, achieving programmable release of payloads with diverse molecular weights at distinct rates typically requires complex polymer designs that can compromise the accessibility and biocompatibility of the delivery system. We present a scalable method for producing injectable, micrometer-scale alginate hydrogel particles (microgels) with precisely tuned microstructures for multiplexed, programmable cargo release. Our approach integrates an established jetting technique with a simple postsynthesis ion-exchange process to fine-tune the cross-linked microstructure of alginate microgels. By varying cation type (Ca^{2+}, Mg^{2+}, Na^{+}) and concentration, we systematically modulate the microgels' chemical and physical properties to control release rates of model compounds, including rhodamine B, methylene blue, and dextrans of various molecular weights. Additionally, a PEG-alginate composite microgel system is used to demonstrate the pre-programmed stepwise release of rhodamine B. These findings offer a straightforward strategy for postsynthetic manipulation of ionic microgels with controllable release performances, paving the way for advanced biomedical applications.

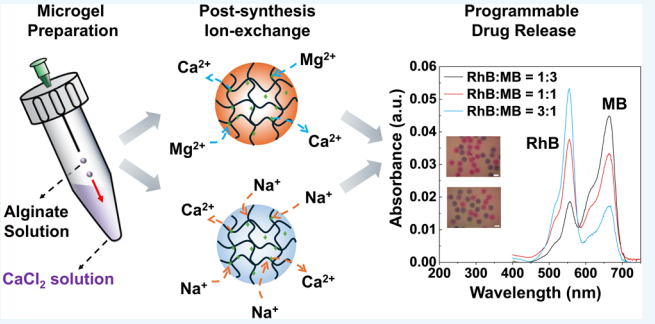

KEYWORDS: *microgels, jet printing, ion exchange, programmable release, release kinetics*

1. INTRODUCTION

Hydrogels, composed of natural or synthetic cross-linked polymers with high water content, have garnered significant attention due to their versatile properties and broad applications. Their structure, maintained by both physical and covalent cross-linking, forms a three-dimensional hydrophilic porous network that enables exceptional water uptake and retention.[1,2] Recent advancements have enabled the preparation of hydrogel particles at the micrometer scale, offering distinct advantages over their bulk counterparts in drug delivery and other therapeutic applications.[3−5] Their small, injectable form factor allows for minimally invasive administration via methods such as percutaneous injections using syringes or catheters.[6] Consequently, these hydrogel microparticles, or microgels, are particularly appealing for programmable drug release because of their injectability, low invasiveness, and high surface area to volume ratio.[3−6] Programmable drug release, in this context, is defined as drug release with desired drug compositions and well-controlled and predetermined release rates. Microgels exhibit remarkable versatility in both physical and chemical characteristics.[6] By combining microgels with different compositions, sizes, and encapsulated contents, tailored material systems can be formulated to meet specific therapeutic needs.[3,6,7] This modularity is especially valuable for managing the complexity of biological processes like development, inflammation, and tissue repair. For instance, microgels can be engineered to provide independently addressable drug delivery rates and multimodal degradation behaviors, paving the way for advanced therapeutic designs.[6] To meet these demands, various fabrication techniques have been developed, including liquid marbles,[8] emulsion-based methods,[9] microfluidics,[10] lithography,[11] and centrifugal-force-driven approaches.[3] Among these, the centrifugal-force-driven method stands out for its ability to produce microgels with high throughput and a narrow size distribution without requiring complex processes or expensive equipment.[11]

Microgels with diameters ranging from 100 to 1000 μm are widely used in controlled drug release, tissue regeneration, and immuno-isolation of therapeutic cells,[13] as their larger size helps reduce foreign-body responses and fibrosis compared to

Received: February 9, 2025
Revised: March 27, 2025
Accepted: April 2, 2025

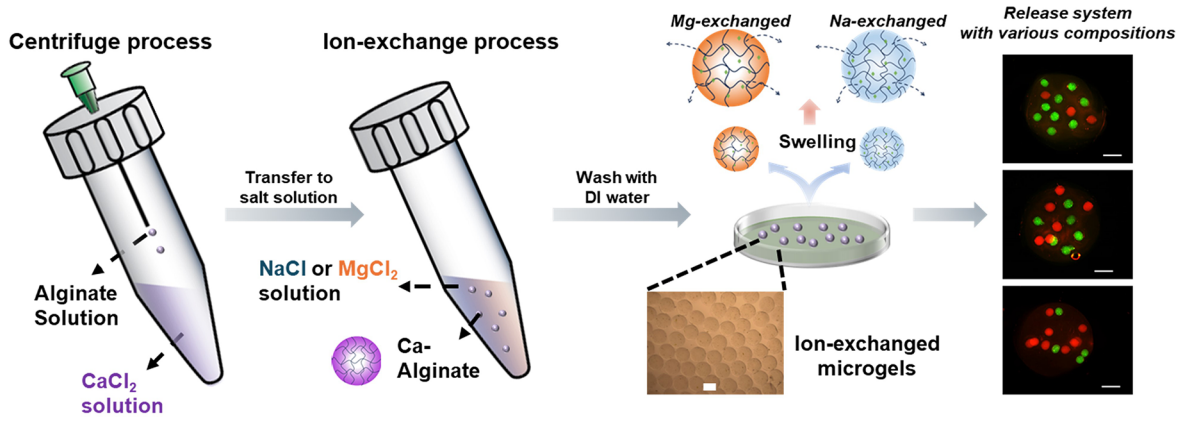

Figure 1. Schematic illustration of the experimental workflow established in this study, including centrifugal-force-driven alginate microgel synthesis, followed by ion-exchange (IX), and subsequent microgel swelling and cargo release. Inset (middle-bottom panel): optical micrograph of as-prepared alginate microgels post IX. Scale bar: 500 μm. Inset (right panels): fluorescent micrographs of a complex delivery system composed of various number ratios of post-IX microgels containing different dye-labeled dextrans (green and red) for multiplexed cargo release. Scale bars: 1000 μm.

smaller particles.[13] Key factors in engineering injectable microgels include the drug release rate and dosage. These parameters depend on the particle's volumetric surface area, mesh size, and the interactions between cargo molecules and the gel matrix.[5,14] Mesh size——the spacing between cross-linked polymer chains——governs liquid uptake and solute diffusion, and is influenced by the polymer chain's molecular weight, the type of cross-linker, and the cross-linking density.[3,5] For example, varying the ratios of stable and cleavable cross-linkers enables compositional control over payload release, as cleavable cross-linkers degrade more rapidly to increase the encapsulant release rate.[6] Other strategies include modifying polymer chains with functional groups to adjust the hydrogel's affinity for encapsulated drugs, further tuning release characteristics.[15] Moreover, incorporating multiple polymer constituents can introduce additional programmability into the microgel release profiles.[7] However, the use of specialty covalent cross-linkers or custom polymer mixtures adds complexity, limits accessibility, and may compromise the biocompatibility of the delivery system. Therefore, it is desirable to develop techniques that fine-tune microgel payload release profiles without the need for additional chemical agents.

Researchers have explored various biopolymers as microgel drug carriers, with alginate attracting significant attention thanks to its hydrophilicity, biocompatibility, and non-immunogenicity.[16,17] Alginate is a linear anionic polysaccharide derived from brown algae or bacteria. It consists of repeating units of β-1,4-linked D-mannuronic acid (M) and L-guluronic acid (G) in varying ratios.[2] Typically, these hydrogels are formed by ionic cross-linking using divalent cations such as Ca^{2+}.[17] The high content of G blocks in alginate facilitates the formation of a rigid polymer network, as each G block binds to two opposing G blocks in an "egg-box" conformation.[1,2] Moreover, alginate hydrogels cross-linked with different ions exhibit distinct gelation characteristics and mechanical properties, providing additional control over the network's mesh size.[17] For example, replacing the divalent cation cross-linker Ca^{2+} with a trivalent Fe^{3+} can produce alginate hydrogel films with enhanced cross-link strength and improved mechanical properties,[18] while reversible cation exchanges—such as those between Ca^{2+} and Zn^{2+}—have been demonstrated in naturally occurring hydrogel systems like cellulose.[19]

In this study, we introduce a generalized strategy to prepare alginate microgels with programmable release profiles via a simple ion-exchange (IX) method (Figure 1). These microgels are formulated using a centrifugal-force-driven technique, initially cross-linked with Ca^{2+},[12,20] and subsequently transferred to various salt solutions for IX. By adjusting the type and concentration of cations used during the IX process, we precisely control the cross-linking density and swollen mesh size of the as-prepared microgels. This approach enables the development of a new class of microgels with tunable release performance that is compatible with payloads of varying molecular weights and charge characteristics, all without resorting to complex cross-linking chemistries and polymer designs. Notably, these alginate microgels with different release profiles can be further combined in modular delivery systems with programmable dosing control, shedding light on new biocompatible routes for engineering microcapsule-based therapeutics for diverse biomedical applications.

2. EXPERIMENTS

2.1. Materials. Sodium alginate (NaAlg), calcium chloride ($CaCl_2$, 96%), magnesium chloride ($MgCl_2$, 98%), sodium chloride (NaCl, 99%), and polyethylene glycol (PEG, M_n = 6 kDa, 20 kDa), rhodamine B (RhB, ≥ 95%), and methylene blue hydrate (MB) were purchased from Sigma-Aldrich Chemicals. Dextran (neutral, M_n = 3 kDa, 70 kDa) was purchased from ThermoFisher. All chemical reagents were used as received without any further purification.

2.2. Preparation of Alginate Microgels. The alginate microgels were prepared by a modified centrifugal-force-driven method (Figure 1). The centrifugal-force-driven modular micronozzle devices were designed based on reported work.[12] In brief, a 23-gauge syringe needle was inserted into a 5 mL centrifuge tube filled with 0.6 mL of aqueous solution with designated compositions. The connection between the tube cap and needle was sealed with epoxy resin to prevent shaking during the centrifuge process. Next, 100 μL of 5 wt % NaAlg aqueous solution was loaded in the needle. The centrifugation was operated at 500 rpm for 5 minutes (min), during which the viscous NaAlg solution was extruded through the micronozzle and formed microdroplets in the solution. For the subsequent ion-exchange (IX) step, after centrifugation, all alginate microgels were first cross-linked in an aqueous solution of $CaCl_2$ for 5 min. These cross-linked alginate microgels were washed with deionized (DI) water, then transferred to a $MgCl_2$ or NaCl aqueous solution and incubated for 3 hours (h). The prepared microparticles were named based on the type of salt used during the IX process ($MgCl_2$ and

https://doi.org/10.1021/cbe.5c00017
Chem Bio Eng. XXXX, XXX, XXX−XXX

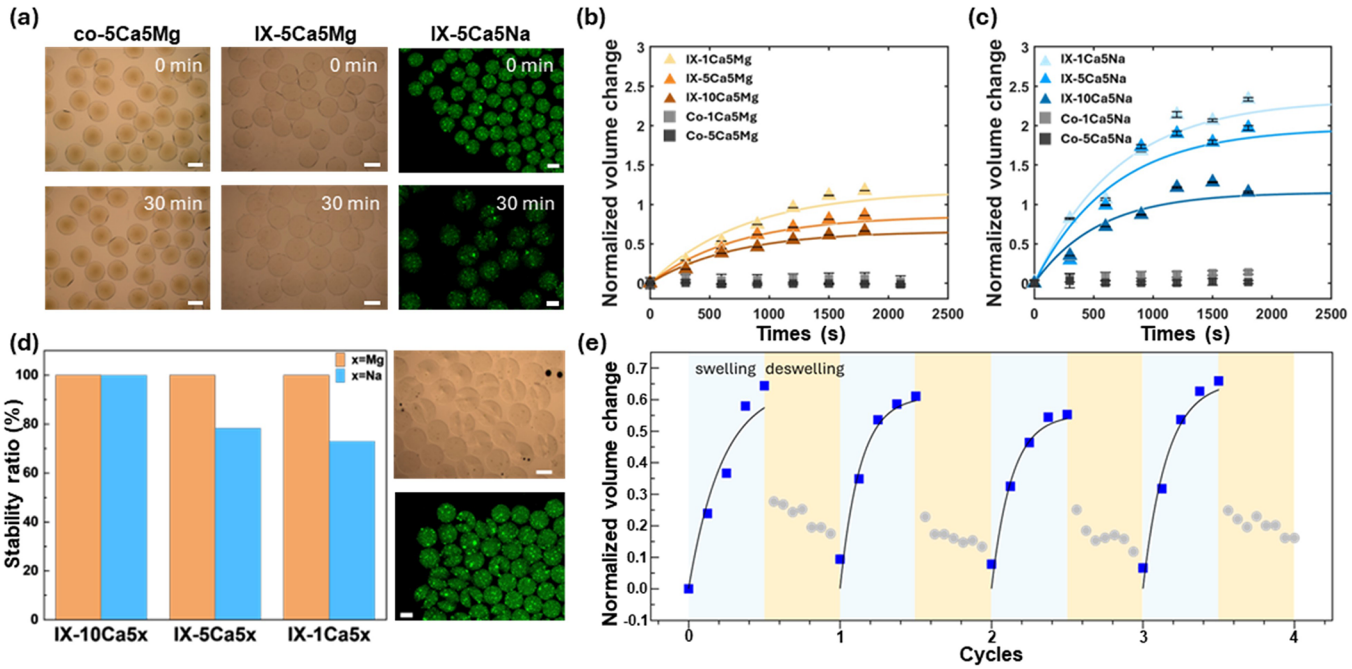

Figure 2. (a) Optical micrographs of 5Ca5Mg microgels prepared by ion-exchange (IX) and co-ion (co) methods, and IX-5Ca5Na before and after swelling for 30 min. Scale bars: 500 μm. (b,c) Normalized volume changes over time of alginate microgels prepared by the IX method (colored) and the co-ion incubation method (gray scale) using (b) $MgCl_2$ (orange) and (c) NaCl (blue). (d) Stability ratios of alginate microgels prepared by the IX method using $MgCl_2$ (orange) and NaCl (blue). Inset panels: representative micrographs of the IX-1Ca5Na microgels that show broken microgels in optical mode (top) and fluorescent mode (bottom). Scale bars: 500 μm. (e) Normalized volume change of the IX-5Ca5Mg microgels during repeated swelling and deswelling cycles. The swelling cycle data are fitted using eq 2. Each data point is taken 5 min apart.

NaCl), and the concentration of $CaCl_2$ during the initial cross-linking step. For instance, if alginate microgels are first collected in a 1 wt % $CaCl_2$ solution and then incubated in a 5 wt % $MgCl_2$ solution, they are labeled as IX-1Ca5Mg. To prepare alginate microgels by the co-ion incubation method, the extruded alginate particles were incubated in co-ion baths containing $CaCl_2$ and $MgCl_2$ or NaCl at different weight ratios (1:5 or 5:5) at room temperature. The nomenclature follows the IX samples, but sample names have co- as prefix instead of IX-. For example, the alginate microgels incubated in co-ion bath containing 1 wt % $CaCl_2$ and 5 wt % NaCl are named co-1Ca5Na. In cases where multiple parallel conditions are consolidated into one sample group, "x" is used to denote the parameter that changes. For instance, "co-xCa5Mg" corresponds to microgels prepared using the co-ion incubation method with various concentrations of $CaCl_2$ and 5 wt % $MgCl_2$ in the incubation solutions.

2.3. Swelling Behavior Analysis. After the IX step, the microgels were washed twice using DI water before being placed on a glass slide under an optical microscope for the swelling tests. DI water was added to initiate swelling. Images of microgels were captured at different time intervals to monitor the size change. The optical micrographs are processed via ImageJ to enhance contrast and locate particle edges, then the particle sizes are extracted using a custom MATLAB script. After the particle radii are identified using the MATLAB script, the radius at time t is divided by the initial radius to obtain the normalized percentage change in radius Δr. The percentage change of volume $\Delta V\%$ is subsequently calculated following the equation: $\Delta V\% = [(1+\Delta r)^3 - 1^3]$, with error propagated as $3*\Delta r^2*\sigma_{\Delta r}$, where σ denotes the standard deviation.

2.4. Single Particle Tracking for Mean Square Displacement (MSD) Measurement. Fluorescent latex beads (diameter = 30 nm) were loaded into the microgels during the jetting process for single particle tracking analysis. Time-dependent trajectories of latex beads within the microparticles were recorded using the Echo Revolve fluorescent microscope and analyzed using ImageJ. Mean square displacement (MSD) values were calculated using an open-source MATLAB code,[21] via the following equation:[21]

$$MSD(\tau) = \langle [r(t+\tau) - r(t)^2] \rangle_t \quad (1)$$

where τ measures the time interval between measurements, $r(t)$ marks the position of the particle at absolute time t, and $\langle\rangle_t$ calculates the temporal average of the argument inside.

2.5. Controlled Cargo Release. To characterize the release process of the as-prepared alginate microgels, RhB, MB and dextrans of different molecular weights were used as model drugs, with RhB and MB loaded into the microgels during the IX process and dextrans loaded along with the NaAlg precursor before cross-linking. The microgels were jetted into $CaCl_2$ solutions as previously described. During IX, the RhB and MB dye molecules were simultaneously infused into the microgels at a non-swelled state via passive diffusion. 0.2 mL of the 5 mg/mL dye stock solutions were added into 10 mL of 5 wt % NaCl or $MgCl_2$ solutions to prepare the 0.1 mg/mL RhB or MB loaded IX solutions, while the 0.2 mg/mL dextrans were mixed into the NaAlg precursor solutions to prepare the dextrans-loaded microgels. After the IX process was completed, a fixed weight of microgels were transferred into 2 mL of DI water to characterize the payload release process. For both RhB and MB, the absorbance of the solution was monitored using UV−vis spectroscopy, whereas for 3 kDa and 70 kDa dextrans, the fluorescent intensity of the microgels was integrated for each microgel particle, upon background noise subtraction.

2.6. Chemical and Morphological Characterizations. The morphology of the prepared microgels was analyzed using field emission scanning electron microscopy (FE-SEM). Elemental mapping was measured using energy dispersive X-ray spectroscopy (EDS, Oxford EDS system). All samples were freeze-dried overnight before the subsequent characterization experiments.

3. RESULTS AND DISCUSSIONS

3.1. Swelling Behavior of Alginate Hydrogel Microgels. Ion cross-linking is a common noncovalent method for establishing a stable network structure in alginate microgels, and the swelling behavior of microgels could be tuned by

https://doi.org/10.1021/cbe.5c00017
Chem Bio Eng. XXXX, XXX, XXX−XXX

Table 1. Fitted Swelling Rate Constants for Different IX-Microgels (Using Eq 2)

	IX-1Ca5Mg	IX-5Ca5Mg	IX-10Ca5Mg	IX-1Ca5Na	IX-5Ca5Na	IX-10Ca5Na
k (s^{-1})	0.00127	0.00136	0.00142	0.00143	0.00152	0.00184
R^2	0.9596	0.9654	0.9816	0.9905	0.9708	0.9654

incorporating different ionic cross-linkers. In addition to the choice of ionic species, we found that the method of cross-linking−−whether by *simultaneous* incubation of multiple ions (i.e., co-ion bath (co)) or by *sequential* exchange of ionic species (i.e., ion-exchange (IX))−−significantly affects the resulted network structure.

Microgels formulated via the co-ion incubation method exhibited a limited swelling ratio (Figure 2b and c). These microgels were prepared using a previously reported centrifugal-force-driven method[12] and were collected in co-ion baths composed of $CaCl_2$ mixed with either $MgCl_2$ or NaCl at different concentrations. We tested mixtures of $CaCl_2$ with $MgCl_2$ or NaCl at weight ratios of 1:5 and 5:5. Upon 3 hours (h) of co-ion incubation, the microgels were transferred to deionized (DI) water for swelling tests, and their diameters were measured over time (Figure 2b and c). Only the samples incubated in a $CaCl_2$-to-NaCl solution at a 1:5 weight ratio (i.e., co-1Ca5Na) exhibited a non-negligible, albeit modest, degree of swelling, while other samples maintained nearly constant size after 40 min of DI water exposure (Figures 2c and S1). After 20 h of swelling, the microgel volumes increased by approximately 52% (i.e., swelling ratio) for the 1 wt % $CaCl_2$ co-ion samples and about 33% for those incubated with 5 wt % $CaCl_2$. Neither the extent nor the rate of swelling was significantly influenced by the co-ion identity (i.e., Mg^{2+} vs. Na^+) (Figure S1b). As a control, microgels cross-linked solely with Ca^{2+} do not swell at all when exposed to DI water (Figure S2). The modest swelling observed in co-ion incubated microgels is attributed to the competition between Mg^{2+} or Na^+ ions with Ca^{2+} for the cross-linking sites within the alginate network. Ca^{2+} ions, due to their stronger affinity with the carboxylate groups, dominate the cross-linking process.[22] As a result, the alginate microgels cross-linked in co-ion baths are chemically similar to those cross-linked with neat $CaCl_2$ solutions at a similar concentration, limiting the applicability of using co-ion incubation for alginate microstructure tuning.

On the other hand, our results suggest that both the swelling rate and final swollen size of the microgels in DI water could be further tuned using the IX method. Microgels subjected to IX exhibited significant swelling within 30 min of DI water exposure (Figures 2b,c and S3). All microgels tested gradually swelled until reaching a size plateau, with their final swollen radii varying based on the type and concentration of salt used during the jetting and subsequent IX processes. Among the $MgCl_2$-exchanged samples, those initially cross-linked in 10 wt % $CaCl_2$ and then subjected to IX in 5 wt % $MgCl_2$ (i.e., IX-10Ca5Mg) swelled less than those cross-linked with 5 wt % $CaCl_2$ (IX-5Ca5Mg), with the 1 wt % $CaCl_2$ cross-linked samples (IX-1Ca5Mg) swelling the most (Figure 2b). This is expected since the higher initial Ca^{2+} concentration in the IX-10Ca5Mg sample limits the extent of Mg^{2+} exchange, thereby preserving Ca^{2+} ions' cross-linking effect, whereas the IX-1Ca5Mg and IX-5Ca5Mg samples start with fewer Ca^{2+} ions. Similarly, the swelling behavior of NaCl-exchanged samples exhibited similar relation with the initial Ca^{2+} cross-linker concentration (Figure 2c). The swelling kinetics can be modeled as a diffusion-dominated process:

$$\frac{Q}{Q_e} = 1 - e^{-kt} \tag{2}$$

assuming that the microgels swell isotropically so that the percent increase in radius translates directly to volumetric expansion. Here, Q measures the percent change in volume at time t, Q_e represents the equilibrium percent change in volume, and k is the swelling rate constant.[23] Comparing the fitted rate constants (Table 1) reveals that the swelling rates differ between the $MgCl_2$- and NaCl-exchanged samples. We attribute this difference to the valency and interaction characteristics of the exchanged cations. Specifically, monovalent Na^+ interacts with only one free carboxylate group, thereby disrupting the strong Ca^{2+} ionic cross-links, whereas Mg^{2+}, although capable of chelating with two carboxylates like Ca^{2+}, preserves the cross-linking effect only partially due to its smaller crystallographic ionic radius. Within each IX group, the initial Ca^{2+} cross-linking density further modulates the swelling rate: samples with higher initial Ca^{2+} content (e.g., IX-10Ca5x) swell the fastest, followed by IX-5Ca5x and then IX-1Ca5x. We speculate that a higher initial Ca^{2+} concentration leads to a faster swelling rate due to greater osmotic pressure difference, but results in a lower equilibrium swelling ratio because of reduced cross-linking density. During the IX process, Mg^{2+} and Na^+ replace Ca^{2+} as cross-linkers in the alginate backbone. The absence of Ca^{2+} in the IX solution sets up an entropic driving force for the chelated Ca^{2+} to dissociate and diffuse out, thereby weakening the cross-linking structure and resulting in larger swelling ratios compared to the co-ion incubation method (Figure 2b and c).

Due to the increased swelling ratio, the boundaries of NaCl-exchanged alginate microgels in DI water become blurred as time progresses. To better visualize their swelling behavior, 30 nm fluorescent PS beads were incorporated into the alginate microparticles, creating clearly defined green fluorescent areas (Figure S3b). Some NaCl-exchanged microgels burst after 30 min of DI water exposure, whereas all $MgCl_2$-exchanged microgels remain intact, demonstrating higher stability (Figure 2d). We define the stability ratio as the number of intact microgels after 30 min of swelling in DI water divided by the total number of microgel particles at the start of the swelling experiment. As expected, microgels cross-linked with a higher initial $CaCl_2$ concentration exhibited a higher stability ratio than those cross-linked with lower $CaCl_2$ concentrations (Figure 2d). For NaCl-exchanged microgels, for instance, the stability ratio decreased from 100% to 73% as the $CaCl_2$ concentration decreased from 10 wt % to 1 wt %. This indicates that the initial $CaCl_2$ cross-linker concentration before IX can be used to fine-tune microgel stability.

The reversibility of swelling behavior in IX-5Ca5Mg microgels was further examined by subjecting them to repeated cycles of swelling in DI water (20 min) followed by deswelling in 5 wt % $CaCl_2$ (30 min). The microgels underwent four complete cycles without significant deterioration in swellability (Figure 2e). After each deswelling cycle, the microgels were transferred to a 5 wt % $MgCl_2$ solution for 1 h to restore their ion-exchanged equilibrium state before returning to DI water

https://doi.org/10.1021/cbe.5c00017
Chem Bio Eng. XXXX, XXX, XXX−XXX

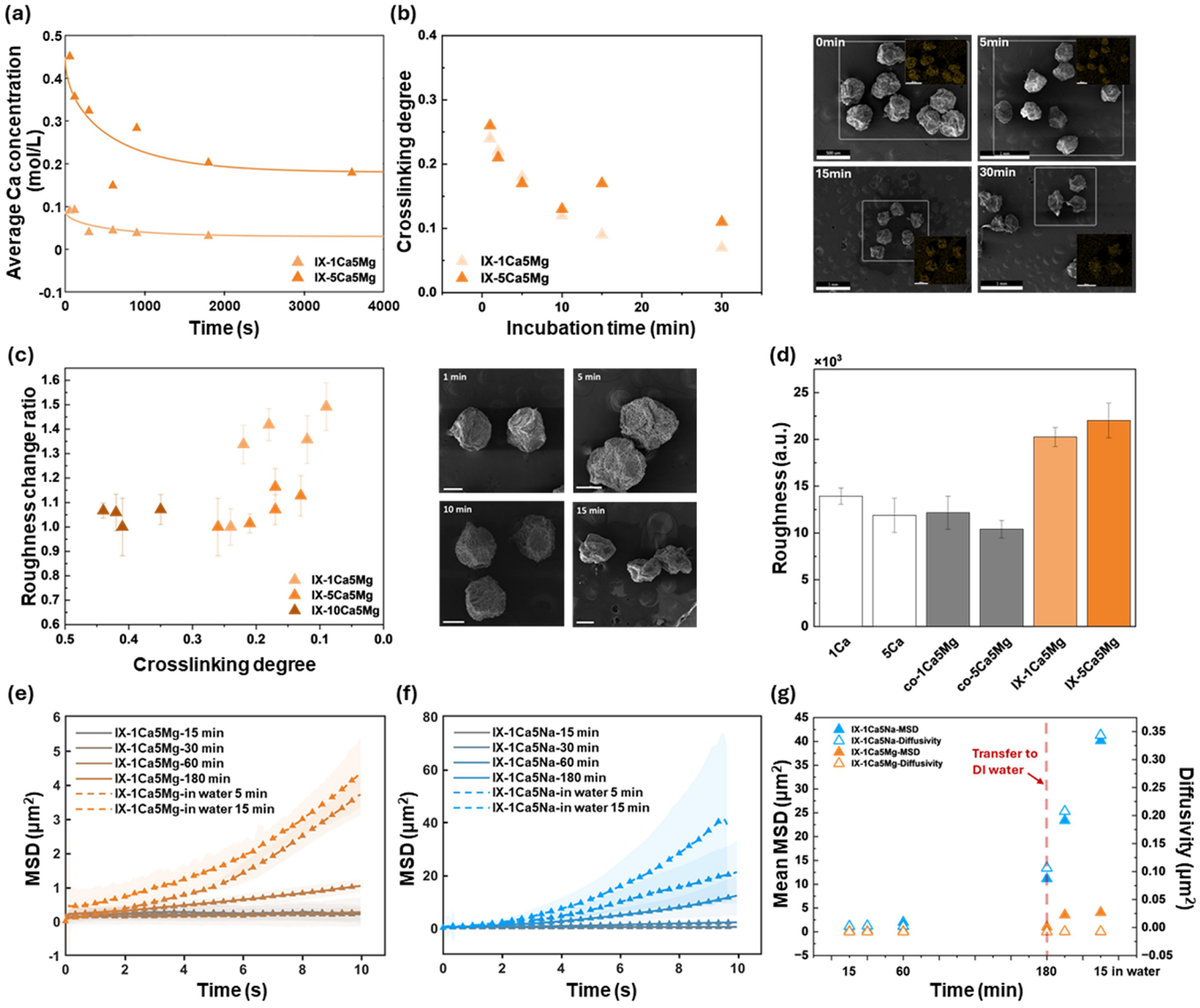

Figure 3. Structure and property changes of alginate microgels prepared via the IX method. (a) Degrees of cross-linking change as a function of incubation time in IX solutions. (b) IX kinetics for the IX-1Ca5Mg and IX-5Ca5Mg samples as measured by the average Ca^{2+} concentration inside the microgels tracked as a function of incubation time. Right panels: representative scanning electron micrographs of freeze-dried IX-1Ca5Mg at different incubation times. Scale bar (0 min): 500 um. Scale bars (5, 15, 30 min): 1 mm. Inset: EDS mapping of Ca signal. Scale Bars: 500 um. (c) Roughness change ratio, defined as relative change in the standard deviations of microgels' pixel intensity analyzed by ImageJ, of the IX-xCa5Mg microgels plotted as a function of the degree of alginate cross-linking, which can be further correlated with incubation time. Error bar represents standard deviation of the roughness change ratio (n = 5). Right panels: representative scanning electron micrographs of freeze-dried IX-1Ca5Mg at different incubation times. Scale bars: 200 μm. (d) Comparison of roughness between microgels prepared by different methods. Error bar represents standard deviation of the pixel intensity fluctuation (n = 5). (e,f) MSD values analyzed using trajectories of 30 nm latex beads in (e) IX-1Ca5Mg and (f) IX-1Ca5Na alginate microgels during the IX process and in DI water. Shaded regions represent the error bars, which are the standard deviations of measured MSD values. (g) The mean MSD values (left ordinate) and calculated diffusivities (right ordinate) change as a function of IX time and exposure time to DI water.

for reswelling. We modeled the percent change in volume using eq 2, which revealed that the swelling rate for the first cycle was significantly slower than in subsequent cycles (Table S1). We speculate that this initial delay results from the jetting process creating highly entangled alginate chains; repeated swelling likely relaxes this entanglement, leading to faster swelling after the first cycle. This reversible swelling−deswelling behavior suggests that ion-exchanged alginate microgels have potential as drug delivery vehicles capable of repeated therapeutic loading and unloading.

3.2. Property Changes of Alginate Microgels during the IX Process. To gain further insight into the IX process, we characterized the structure−property relations induced by IX with Na^+ and Mg^{2+}. We performed morphological and elemental analyses on $MgCl_2$-exchanged samples using scanning electron microscopy (SEM) and energy dispersive X-ray spectroscopy (EDS) mapping to elucidate how the cross-linking density and microgel morphology evolve during IX. Specifically, we analyzed changes in the Ca^{2+}, Mg^{2+} and O contents of the IX-xCa5Mg microgels (where x = 1, 5) at various incubation times (Figure S4 and Table S2). The alginate content was estimated from the oxygen level using the stoichiometric relation: alginate% = O%/6. As expected, no Mg^{2+} signal was detected in microgels incubated solely in

https://doi.org/10.1021/cbe.5c00017
Chem Bio Eng. XXXX, XXX, XXX−XXX

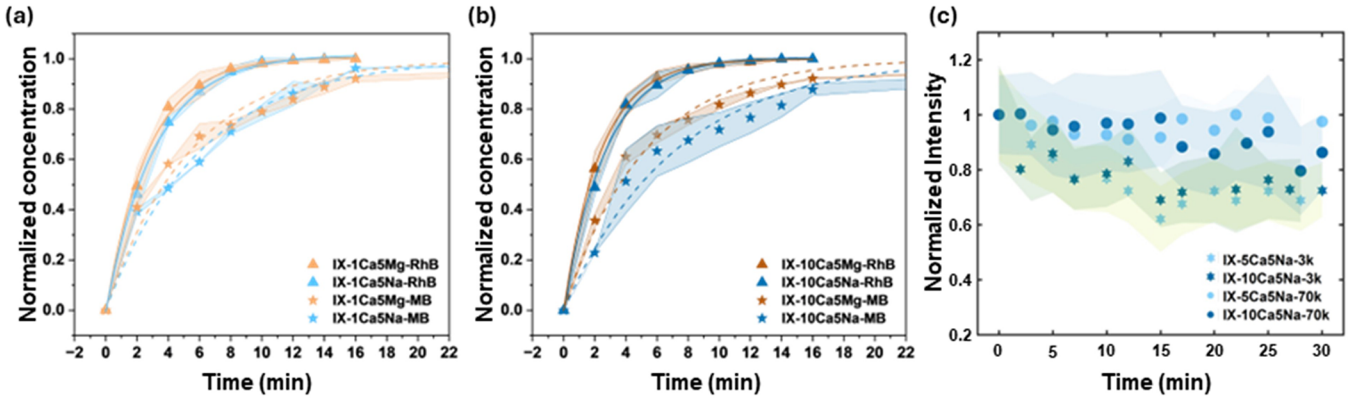

Figure 4. (a,b) Cargo release profiles of RhB and MB from the (a) IX-1Ca5x and (b) IX-10Ca5x samples (x = Mg or Na). Shaded regions represent the error bars, which are the standard deviations in the measured concentrations (n = 3). Dotted and solid lines represent the fitted release profiles using eq 5. (c) Cargo release profiles of 3 kDa and 70 kDa dextrans from the IX-xCa5Na microgels (x = 5 or 10). Shaded regions represent the error bars, which are the standard deviations in measured fluorescent intensities (n = 3).

$CaCl_2$, and the Ca^{2+} content decreased as IX progressed. The degree of cross-linking——calculated from the Ca^{2+} to alginate ratio——decreased with increasing IX time, reaching a plateau after 10 min (Figure 3a). Additionally, particles prepared via the co-ion incubation method exhibited significantly higher degrees of cross-linking (Figure S5). For a quantitative assessment, we modeled the IX process as Fickian diffusion, considering that the ionic radii are relatively small compared to the average pore size of the alginate hydrogel network.[24] We assumed that the IX reaction rate is fast enough that the overall process is transport-limited. In eq 3, RCa represents chelated Ca^{2+}, while free Ca^{2+} ions are denoted as Ca^{2+}. In eq 4, $[Ca^{2+}]$ represents the free Ca^{2+} concentration at space-time (r, t), where r measures the radial distance from the microgel center, and t is the elapsed time. We experimentally determined and added $[Ca^{2+}]_\infty$, the concentration of the residually bound Ca^{2+} inside the microgel after all the "free" Ca^{2+} ions have diffused out, to the fitted $[Ca^{2+}]$ profile to account for the chemical equilibrium between the chelated Ca^{2+} and Mg^{2+} (see Section S2C for details).

$$RCa + Mg^{2+} \leftrightarrow RMg + Ca^{2+} \tag{3}$$

$$\frac{\partial[Ca^{2+}]}{\partial t} = D\frac{1}{r^2}\frac{\partial}{\partial r}\left(r^2\frac{\partial[Ca^{2+}]}{\partial r}\right) \tag{4}$$

This simple model provides an excellent fit to the experimental data (Figure 3b). The fitted diffusion coefficients for the interior (D_i) and exterior (D_e) of the microgels are as follows: for IX-1Ca5Mg, $D_i = 1.76 \times 10^{-11}$ m^2/s; for IX-5Ca5Mg, $D_e = 1.14 \times 10^{-10}$ m^2/s; $D_i = 1.69 \times 10^{-11}$ m^2/s; $D_e = 1.11 \times 10^{-10}$ m^2/s. These diffusivities are consistent with reported literature values[24] and indicate no significant differences between the IX-1Ca5Mg and IX-5Ca5Mg samples.

The degree of hydrogel cross-linking is known to affect its structural rigidity.[25] As IX progresses, the microgels' elastic modulus decreases, resulting in elevated surface roughness (due to increased gel buckling) upon freeze-drying.[26] This is evident from the observed intensity fluctuations in the corresponding scanning electron micrographs (Figure S6). With increasing IX time in $MgCl_2$ (which corresponds to less Ca^{2+}–alginate cross-links) or with lower initial $CaCl_2$ concentrations, the freeze-dried microgels buckle more easily, leading to increased surface roughness (Figure 3c). In contrast, microgels prepared via the co-ion incubation method or cross-linked in pure $CaCl_2$ solutions (without IX) exhibit much smoother surface morphologies (Figure 3d). Taken together, these results suggest that the ion-exchanged alginate microgels possess fewer Ca^{2+}–alginate cross-links than those prepared by co-ion incubation or non-IX controls, resulting in weaker internal microgel networks, faster swelling rates, and greater swellability in DI water.

Modulating the cross-linking strength and density via the IX process also affects the diffusion properties within the alginate microgels. We evaluated these properties by measuring the Mean Square Displacement (MSD) of encapsulated tracer nanoparticles (Figure 3e–g).[21] Specifically, single particle tracking was used to monitor the MSD of 30 nm fluorescent latex beads in alginate microgels at various stages of IX. Twenty hydrogel microgels containing latex beads (cross-linked in 1 wt % $CaCl_2$) were transferred into a microfluidic device (Figure S7a), and $MgCl_2$ or NaCl solution was introduced to initiate the respective IX processes in situ. The movement of the encapsulated latex beads was recorded using a fluorescent microscope, and the MSD values of microgels incubated in IX solution for different times were plotted as a function of time interval between measurements (Figure 3e and f). For controls, we measured the MSD of latex beads in non-cross-linked alginate aqueous solution and in a neat Ca^{2+}-cross-linked alginate gel without IX (Figure S7b). The fluorescent beads exhibited rapid movement in the non-cross-linked alginate, whereas samples cross-linked with 1 wt % $CaCl_2$ showed a drastic reduction in MSD——only about one-tenth of that observed in the non-cross-linked system (Figure S7b). Furthermore, exposure of Ca^{2+}-cross-linked alginate samples to DI water for 3 h did not significantly alter the mean MSD values, consistent with our previous observation that the pure Ca^{2+}-cross-linked alginate microgels do not swell (Figure S2).

On the other hand, the MSD values of the IX-1Ca5Mg and IX-1Ca5Na samples increased monotonically with IX time, reflecting a decrease in cross-linking density during the IX process (Figure 3g). Notably, NaCl-exchanged microgels showed a more pronounced increase in mean MSD values compared to their $MgCl_2$-exchanged counterparts, indicating that they possess weaker cross-links——consistent with our EDS mapping results. After IX was completed, the ionic solutions were removed and replaced with DI water, which

https://doi.org/10.1021/cbe.5c00017
Chem Bio Eng. XXXX, XXX, XXX–XXX

Table 2. Fitted Release Rates k, Terminal Concentration C_∞, and Fitting Parameter A for (a) RhB and (b) MB Release of Ion-Exchanged Microgels

(a) RhB

Samples	IX-1Ca5Mg	IX-1Ca5Na	IX-10Ca5Mg	IX-10Ca5Na	IX-1Ca5Mg-24h	IX-1Ca5Na-24h	1Ca	10Ca
k (min^{-1})	0.37 ± 0.018	0.32 ± 0.010	0.36 ± 0.0056	0.36 ± 0.022	0.47 ± 0.016	0.33 ± 0.035	0.36 ± 0.035	0.46 ± 0.024
C_∞ (mg/mL)	0.00246	0.00200	0.00279	0.00209	0.0099	0.0098	0.00272	0.00277
A	−0.0018	−0.0012	−0.0020	−0.0013	−0.00056	−0.00050	−0.0017	−0.0019

(b) MB

Samples	IX-1Ca5Mg	IX-1Ca5Na	IX-10Ca5Mg	IX-10Ca5Na
k (min^{-1})	0.21 ± 0.029	0.14 ± 0.022	0.22 ± 0.022	0.18 ± 0.040
C_∞ (mg/mL)	0.000687	0.000498	0.000703	0.00455
A	−0.00055	−0.00030	−0.00056	−0.00027

induced further swelling and changes in the microgel diffusion properties. Both $MgCl_2$- and NaCl-exchanged microgels experienced a dramatic increase in mean MSD values due to rapid swelling, with a greater increase observed in the NaCl-exchanged samples (Figure 3g). The linear portion of the MSD data was used to calculate the tracer particle diffusivities in a three-dimensional system (Figures 3g and S8), although diffusivities may vary for other small molecular cargos depending on their size and charge. These results suggest that the IX process provides a new set of engineering handles to fine-tune cargo diffusivity within ion cross-linked alginate microgels in a facile and biocompatible manner, without resorting to complex chemical reactions.

3.3. Cargo Release Performance of the IX Alginate Microgels. To evaluate the potential of using IX to fine-tune the drug delivery performance of alginate microgels, we investigated the release properties of various model compounds encapsulated in the microgels. The effect of cargo size was assessed by encapsulating molecules of increasing size—rhodamine B (RhB), 3 kDa dextran, and 70 kDa dextran—either during jet printing or during the IX process. The microgels were then exposed to DI water to initiate the diffusive release of the payloads. Calibration curves for RhB and methylene blue (MB) were obtained via UV−vis absorption measurements (Figure S9), and the normalized concentration (for RhB) or fluorescent intensity (for dextran) was monitored over time (Figure 4). The payload release follows first-order kinetics, described by the equation:

$$C(t) = C_\infty + Ae^{-kt} \quad (5)$$

For small molecular cargos such as RhB, there was no significant difference in the measured release rates between the IX-1Ca5x and IX-10Ca5x microgels (where x = Mg or Na; Table 2). However, an interesting, albeit subtle, trend emerged: samples that swelled more exhibited slower release rates. This trend was observed when comparing the NaCl- and $MgCl_2$-exchanged microgels (i.e., IX-1Ca5x and IX-1Ca5x-24h), and the 1Ca and 10Ca controls (no IX).. We attribute this behavior to (1) differences in the osmotic pressure within the microgels, and (2) the density of free carboxylate groups within the alginate network. At the neutral pH used in our release studies, RhB is slightly cationic; thus, a higher free carboxylate content leads to stronger electrostatic interactions with the negatively charged alginate backbone, slowing the release. At the same time, a higher free carboxylate content indicates reduced cross-linking, allowing for increased swelling. However, because RhB is small relative to the network's mesh size, the matrix expansion from swelling does not significantly enhance its diffusion, resulting in this counterintuitive trend. This cargo-alginate electrostatic interaction is further amplified when using MB, which has additional positively charged functional groups. Consequently, MB exhibits a slower overall release rate, with NaCl-exchanged microgels releasing MB more slowly than $MgCl_2$-exchanged ones (Figure 4a and b).

The release of larger molecular payloads—namely 3 kDa and 70 kDa dextrans—was studied using the IX-xCa5Na samples (where x = 5 or 10) (Figure 4c). Note that the normalized intensity starts at 1 rather than 0 because the data tracks the fluorescent intensity of the microgels, not the surrounding solution. The release rate of 3 kDa dextran was significantly slower than that of RhB and MB, and no significant difference can be observed between microgels with different initial Ca^{2+} concentrations. When the molecular weight was increased to 70 kDa, virtually no cargo was released over a similar time scale (Figure 4c). These results suggest that both the molecular size of the payload and its state of charge play an important role in determining the release rate.

3.4. Complex Release System Based on Multiple Alginate Microgels. The IX alginate microgels can be combined into ensemble mixtures that encapsulate different molecules, enabling diverse release profiles within a single drug delivery system. To demonstrate this versatility, we used RhB and MB as model drugs with IX-1Ca5Mg microgels as the carrier. All microgel subpopulations were prepared using the method described in Section 2.5. Microgels encapsulating RhB and MB were prepared separately and then mixed at different weight ratios while maintaining a constant total weight of 20 mg. The deconvoluted release profiles reveal a slightly lower encapsulation efficiency for MB compared to RhB, as indicated by the terminal dye concentrations, which align with the weight ratios of the two microgel constituents (Figure 5a). Increasing the proportion of MB-containing microgels led to a higher absorption peak intensity of MB in the supernatant and a corresponding decrease in the RhB peak, as expected (Figure 5b). Importantly, the release rates of RhB and MB remained consistent with those measured the individual release experiments (Figure 5c). These results suggest that the release of multiple payloads in a single system can be controlled by adjusting the ratios of microgels encapsulating them.

Furthermore, we demonstrate that multiplexed IX alginate microgels can be used to program complex temporal release behavior for a single cargo. To illustrate this, we selected RhB as the model drug and encapsulated it in various IX-microgels. The alginate microgels were prepared using different cations during the IX step, and subsequently mixed at varying ratios to form a complex release system. In these experiments, the as-prepared microgels were coated with a polyethylene glycol

https://doi.org/10.1021/cbe.5c00017
Chem Bio Eng. XXXX, XXX, XXX−XXX

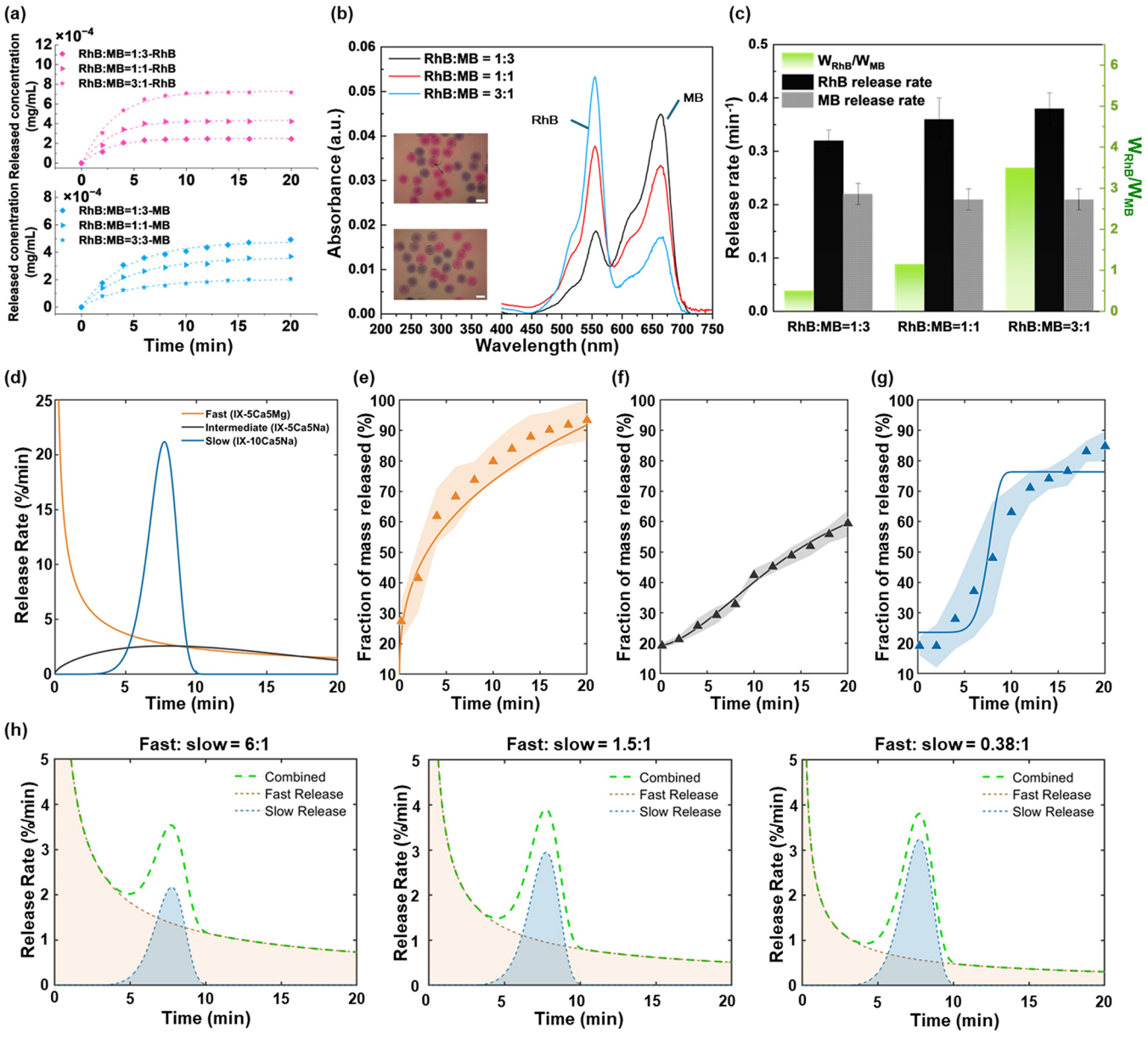

Figure 5. Complex release systems multiplexing different ion-exchanged microgels. (a) Deconvoluted release profiles of RhB (magenta) and MB (cyan) from three microgel systems consisting of different compositions of the IX-1Ca5Mg microgels preloaded with either RhB or MB. Dotted lines represent the best fits from eq 5. (b) Representative UV−vis spectra of the RhB and MB payloads released from the three microgel compositions used in (a) at 20 min of release. Inset: optical micrographs of microgels encapsulated with different dyes mixed in different compositions. Scale bars: 500 μm. (c) Fitted payload release rate constants (left ordinate) for both RhB and MB, as well as the ratios of the weight of RhB-encapsulated microgels (W_{RhB}) to that of MB-encapsulated microgels (W_{MB}) (right ordinate) for all three microgel compositions tested in (a). Error bars represent standard deviations of presented data (n = 3). (d) Fitted release rates as a function of time and the corresponding (e−g) release profiles for the fast- (IX-5Ca5Mg), intermediate- (IX-5Ca5Na), and slow- (IX-10Ca5Na) releasing microgels. Shaded regions represent the error bars, which is the standard deviations of presented data (n = 3). (h) Fitted release rates of three microgel compositions consist of the fast-releasing regime (orange) and a slow-releasing one (blue).

(PEG) layer to further retard drug release and to help distinguish the differences in RhB diffusion rates among the various IX-microgel populations (Figure S10a).[27] To optimize the coating composition, PEG with different molecular weights was added to the IX solution at a total concentration of 5 wt %, while all other procedures remained unchanged. SEM images revealed that the PEG-coated microgels exhibited a smoother surface than the uncoated ones (Figure S10b). Next, we measured the release profiles of various PEG-coated IX-10Ca5Na microgels (Figure S10c). The microgels coated with a mixture of PEG at a 1:3 ratio (6 kDa to 20 kDa) exhibited a significantly delayed release profile and was used for all subsequent experiments. To quantitatively describe the release process, the overall temporal concentration profile was deconvoluted into two regimes by combining the modified Korsmeyer-Peppas model for burst or sustained release (eq 6) with the Weibull model for delayed release (eq 7).[28−30]

$$\frac{M(t)}{M_\infty} = k \times t^n + C_1 \tag{6}$$

https://doi.org/10.1021/cbe.5c00017
Chem Bio Eng. XXXX, XXX, XXX−XXX

where $M(t)$ is the mass of model drug released at time t, M_∞ is the final equilibrium released mass of drug, k is the rate constant, n is the release exponent,[31] and C_1 is a fitting constant.

$$\frac{M(t)}{M_\infty} = D \times (1 - \exp(-\alpha \times t^{\beta})) + C_2 \quad (7)$$

where D is the amplitude scaling factor, α is the apparent release constant,[28] β is the shape factor,[28] and C_2 is a fitting constant.

The first-order time derivatives of the release profiles for IX-5Ca5Mg, IX-5Ca5Na, IX-10Ca5Na microgels−−reflecting their respective cargo release rates−−exhibit peaks at different times, highlighting the potential of the microgel platform in formulating multiplexed systems with tunable release times for a single drug payload (Figure 5d−g and Table S3).[31] We fitted the RhB release profile for the fast-releasing IX-5Ca5Mg microgels using the Korsmeyer-Peppas model and obtained an n value of 0.339, which is lower than expected for non-Fickian diffusion processes (Figure 5e).[5] This suggests that RhB release in IX-5Ca5Mg microgels is not hindered by interactions with the gel matrix.[5] To demonstrate the feasibility of a complex drug delivery system with tunable release times for a single payload, we combined a pair of the fast-releasing (IX-5Ca5Mg) and slow-releasing (IX-10Ca5Na) microgels. The total number of microgels in each delivery system was kept constant while varying the ratios of these two subpopulations to program the desired release profile (Figure 5h). The overall release profile exhibits two distinct stages (Figure S11) and can be modeled as a linear combination of the Korsmeyer-Peppas and the Weibull equations for individual components:

$$\frac{M(t)}{M_\infty} = S \times D \times (1 - \exp(-\alpha \times t^{\beta})) + F \times k \times t^{n} + C_3 \quad (8)$$

where S and F are the coefficients corresponding to the proportions of slow- and fast-releasing microgels (Table 3). C_3 is a fitting constant, and the parameters α, β, n, D and k are obtained from eqs 6 and 7 (Table S3).

Table 3. Fitted Coefficients for Three Complex Delivery Systems Consisting of Various Ratios of Fast- to Slow-Releasing Microgels

Experimental ratio of fast- and slow-release samples	S* D	F* k	S	F	Calculated ratio of fast- and slow-release samples (ratio of F to S)
6:1	5.402	15.649	0.102	0.494	4.83:1
1.5:1	7.361	10.894	0.139	0.344	2.46:1
0.38:1	8.072	6.488	0.153	0.205	1.34:1

As expected, reducing the ratio of fast- to slow-releasing microgels leads to a corresponding decrease in the fitted S-to-F ratio (Table 3). To visualize the separate contributions of the two subpopulations, we decoupled the overall payload release rate (calculated from the first-order time derivative of the combined release profile) into fast-releasing (orange) and slow-releasing regimes (blue) (Figure 5h). As the ratio of fast-to-slow microgels decreases, the area underneath the fast-releasing curve diminishes, while the slow-releasing contribution increases. Together, these results demonstrate that programmable cargo release can be achieved by tuning the proportions of alginate microgel subpopulations with customizable release profiles via controlled IX.

4. CONCLUSION

We have developed a scalable method for preparing alginate hydrogel microparticles with programmable release profiles using an in situ ion-exchange (IX) approach. The microgels were fabricated via a centrifugal force-driven technique and initially cross-linked in $CaCl_2$, before being transferred into $MgCl_2$ or NaCl solutions for IX. By systematically adjusting the $CaCl_2$ concentration and varying both the type and concentration of the salt during the IX process, we precisely modulated the swelling behavior and cross-linking density of the microgels, thereby controlling the diffusivity and release rate of encapsulated payloads. This method produced microgels with distinct release profiles tailored to model compounds of varying molecular weights and charges. Moreover, by combining different types of microgels in adjustable ratios, we demonstrated the modularity of our system, enabling the design of complex release platforms that offer a spectrum of rapid and sustained release characteristics. These findings underscore the potential of our approach to create versatile, biocompatible delivery systems for a wide range of biomedical applications.

■ ASSOCIATED CONTENT

Supporting Information

The Supporting Information is available free of charge at https://pubs.acs.org/doi/10.1021/cbe.5c00017.

Optical micrographs of alginate microgel swelling behavior and analysis, elemental and morphology analysis of alginate microgels, single particle tracking for Mean Square Displacement (MSD) analysis, complex release performance (PDF)

■ AUTHOR INFORMATION

Corresponding Author

Albert Tianxiang Liu − *Department of Chemical Engineering, Department of Materials Science and Engineering, and Biointerfaces Institute, University of Michigan, Ann Arbor, Michigan 48109, United States;* orcid.org/0000-0001-8854-5854; Phone: +1-734-763-5192; Email: atliu@umich.edu

Authors

Rong Ma − *Department of Chemical Engineering, University of Michigan, Ann Arbor, Michigan 48109, United States*

Jihpeng Sun − *Department of Chemical Engineering, University of Michigan, Ann Arbor, Michigan 48109, United States*

Sungwan Park − *Department of Chemical Engineering, University of Michigan, Ann Arbor, Michigan 48109, United States*

Fiona Nikolla − *Department of Chemical Engineering, University of Michigan, Ann Arbor, Michigan 48109, United States*

Complete contact information is available at: https://pubs.acs.org/10.1021/cbe.5c00017

Author Contributions

¶R.M. and J.S. contributed equally.

Notes

The authors declare no competing financial interest.

■ ACKNOWLEDGMENTS

We acknowledge the support from the National Science Foundation (Grant Number: 2243104, Center for Complex Particle Systems, COMPASS) and the American Chemical Society Petroleum Research Fund (Grant Number: 66979-DNI10). We thank the Michigan Materials Research Institute (MMRI) and the University of Michigan's Michigan Center for Materials Characterization via an NSF grant (DMR-1625671), which supports the SEM resources that were utilized in this work.

■ REFERENCES

(1) Hernández-González, A. C.; Téllez-Jurado, L.; Rodríguez-Lorenzo, L. M. Alginate hydrogels for bone tissue engineering, from injectables to bioprinting: A review. *Carbohydr. Polym.* **2020**, *229*, No. 115514.
(2) Zhang, M.; Zhao, X. Alginate hydrogel dressings for advanced wound management. *Int. J. Biol. Macromol.* **2020**, *162*, 1414−1428.
(3) Daly, A. C.; Riley, L.; Segura, T.; Burdick, J. A. Hydrogel microparticles for biomedical applications. *Nat. Rev. Mater.* **2020**, *5*, 20−43.
(4) Agrawal, G.; Agrawal, R. Functional Microgels: Recent Advances in Their Biomedical Applications. *Small* **2018**, *14*, No. 1801724.
(5) Li, J.; Mooney, D. J. Designing hydrogels for controlled drug delivery. *Nat. Rev. Mater.* **2016**, *1*, 1−17.
(6) Mealy, J. E.; et al. Injectable Granular Hydrogels with Multifunctional Properties for Biomedical Applications. *Adv. Mater.* **2018**, *30*, No. 1705912.
(7) Cong, Z.; et al. A novel controlled drug delivery system based on alginate hydrogel/chitosan micelle composites. *Int. J. Biol. Macromol.* **2018**, *107*, 855−864.
(8) Bielas, R.; et al. Biocompatible Hydrogel-Based Liquid Marbles with Magnetosomes. *Materials* **2024**, *17*, 99.
(9) Lan, Y.; et al. Pickering emulsion-embedded hierarchical solid-liquid hydrogel spheres for static and flow photocatalysis. *J. Colloid Interface Sci.* **2021**, *589*, 587−596.
(10) Zheng, Y.; et al. Scalable Production of Biomedical Microparticles via High-Throughput Microfluidic Step Emulsification. *Small* **2023**, *19*, No. 2206007.
(11) Jang, W.; et al. Direct functionalization of cell-adhesion promoters to hydrogel microparticles synthesized by stop-flow lithography. *J. Polym. Sci.* **2022**, *60*, 1767−1777.
(12) Kang, S.-M.; Lee, G.-W.; Huh, Y. S. Centrifugal Force-Driven Modular Micronozzle System: Generation of Engineered Alginate Microspheres. *Sci. Rep* **2019**, *9*, 12776.
(13) Veiseh, O.; et al. Size- and shape-dependent foreign body immune response to materials implanted in rodents and non-human primates. *Nat. Mater.* **2015**, *14*, 643−651.
(14) Mo, C.; Luo, R.; Chen, Y. Advances in the Stimuli-Responsive Injectable Hydrogel for Controlled Release of Drugs. *Macromol. Rapid Commun.* **2022**, *43*, No. 2200007.
(15) Jaklenec, A.; et al. Sequential release of bioactive IGF-I and TGF-β1 from PLGA microsphere-based scaffolds. *Biomaterials* **2008**, *29*, 1518−1525.
(16) Zhang, X.; et al. Role of a high calcium ion content in extending the properties of alginate dual-crosslinked hydrogels. *Journal of Materials Chemistry A* **2020**, *8*, 25390−25401.
(17) Hu, C.; Lu, W.; Mata, A.; Nishinari, K.; Fang, Y. Ions-induced gelation of alginate: Mechanisms and applications. *Int. J. Biol. Macromol.* **2021**, *177*, 578−588.
(18) Ji, D.; et al. Superstrong, superstiff, and conductive alginate hydrogels. *Nat. Commun.* **2022**, *13*, 3019.
(19) Zhou, S.; et al. Cellulose Hydrogels by Reversible Ion-Exchange as Flexible Pressure Sensors. *Advanced Materials Technologies* **2020**, *5*, No. 2000358.
(20) Eral, H. B.; et al. Governing Principles of Alginate Microparticle Synthesis with Centrifugal Forces. *Langmuir* **2016**, *32*, 7198.
(21) Rose, K. A.; et al. Nanoparticle dynamics in hydrogel networks with controlled defects. *Soft Matter* **2022**, *18*, 9045−9056.
(22) Topuz, F.; Henke, A.; Richtering, W.; Groll, J. Magnesium ions and alginate do form hydrogels: a rheological study. *Soft Matter* **2012**, *8*, 4877−4881.
(23) Yavari, N.; Azizian, S. Mixed diffusion and relaxation kinetics model for hydrogels swelling. *J. Mol. Liq.* **2022**, *363*, No. 119861.
(24) Teixeira, V. F. T.; et al. Ion exchange kinetics of magnetic alginate ferrogel beads produced by external gelation. *Carbohydr. Polym.* **2014**, *111*, 198−205.
(25) Henderson, K. J.; Zhou, T. C.; Otim, K. J.; Shull, K. R. Ionically Cross-Linked Triblock Copolymer Hydrogels with High Strength. *Macromolecules* **2010**, *43*, 6193−6201.
(26) Zhou, C.; et al. Hydrogel platform with tunable stiffness based on magnetic nanoparticles cross-linked GelMA for cartilage regeneration and its intrinsic biomechanism. *Bioactive Materials* **2023**, *25*, 615−628.
(27) Sarmadi, M.; et al. Experimental and computational understanding of pulsatile release mechanism from biodegradable core-shell microparticles. *Science Advances* **2022**, *8*, No. eabn5315.
(28) Wickremasinghe, N. C.; Kumar, V. A.; Hartgerink, J. D. Two-Step Self-Assembly of Liposome-Multidomain Peptide Nanofiber Hydrogel for Time-Controlled Release. *Biomacromolecules* **2014**, *15*, 3587−3595.
(29) Korsmeyer, R. W.; Gurny, R.; Doelker, E.; Buri, P.; Peppas, N. A. Mechanisms of solute release from porous hydrophilic polymers. *Int. J. Pharm.* **1983**, *15*, 25−35.
(30) Costa, P.; Sousa Lobo, J. M. Modeling and comparison of dissolution profiles. *European Journal of Pharmaceutical Sciences* **2001**, *13*, 123−133.
(31) Dash, S.; Murthy, P. N.; Nath, L.; Chowdhury, P. Kinetic modeling on drug release from controlled drug delivery systems. *Acta Polym. Pharm.* **2010**, *67* (3), 217−223.

https://doi.org/10.1021/cbe.5c00017
Chem Bio Eng. XXXX, XXX, XXX−XXX